Numerical Model of a Magnetically Enhanced Plasma Thruster

IEPC-2019-415

Presented at the 36th International Electric Propulsion Conference
University of Vienna, Austria
September 15-20, 2019

M. Magarotto* and D. Pavarin†
University of Padova, Via 8 Febbraio 1848, 2, 35122, Padova, Italy

M. Manente‡ and F.Trezzolani§
Technology for Propulsion and Innovation S.r.l., Via Altinate, 125, 35121, Padova, Italy

Abstract: This work is devoted to the presentation of a numerical model of a Helicon Plasma Thruster which relies on: (i) the 3-Dimensional adVanced fluId dRifT diffUsion plaSma solver (3D-VIRTUS) for the simulation of the Plasma Source, and (ii) an analytical model of the plume for the solution of the plasma acceleration and detachment, and in turn for the preliminary estimation of the propulsive performances (e.g., thrust and specific impulse). In particular the results of the numerical model have been compared against experimental measurements performed with a thrust stand in order to evaluate the reliability of the code when dealing with real-life prototypes. Therefore, a dedicated combined numerical-experimental campaign has been conducted on a non-optimized low power (50-W range) HPT prototype operated with argon propellant.

I. Introduction

The research activity in the electric propulsion field is today very active even though mature technologies as Ion and Hall-effect thrusters have been employed in space missions for years.[1] In the last decade, particular effort has been paid in the development and study of a new concept of magnetically enhanced plasma thrusters system called Helicon Plasma Thrusters (HPTs).[2] A HPT is composed of a Helicon plasma source at its core for the plasma generation,[3] and a magnetic nozzle which accelerates the exhaust stream and, ultimately, produce thrust.[4] A schematic of a HPT has been reported in Fig. 1, that encompasses: (i) the dielectric tube inside which the neutral gas is ionized; (ii) the Radio Frequency (RF) antenna that works in the MHz range, and produces the EM fields for plasma generation and heating; (iii) the magnets (permanent or electromagnets) that generate a magneto-static field with divergent field lines in the magnetic nozzle region. The purpose of the magneto-static field is three-fold: (i) to enhance the plasma confinement, (ii) to allow for the propagation of whistler waves[5,6] within the source, and (iii) to provide the magnetic nozzle effect that guides, expands and accelerates a plasma jet into vacuum. HPTs present a number of interesting features, namely: (i) a very simple structure and, in turn, a low cost; (ii) absence of electrodes immersed in the plasma, with consequently limited erosion and long life; (iii) no need for a neutralizer[7] because the ejected stream is a globally neutral plasma and not an ion beam; (iv) good power scalability;[8,9] (v) good adaptability to different propellants without geometric reconfiguration.[9]

HPTs have been studied, and developed in many international projects by both research centres and companies. At Astra Rocket Company has been involved in the VASIMR project, which aims at the development

*Research Fellow, Centro di Ateneo di Studi e Attività Spaziali "Giuseppe Colombo" - CISAS, magamir91@gmail.com mirko.magarotto@unipd.it
†Associate Professor, Department of Industrial Engineering - DII, daniele.pavarin@unipd.it
‡Plasma propulsion manager, m.manemte@t4innovation.com
§Senior R&D Engineer, f.trezzolani@t4innovation.com

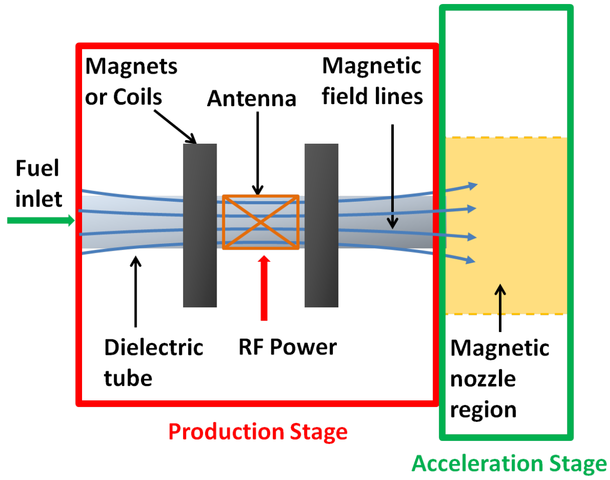

Figure 1. Schematic of a HPT which highlights the separation between *Production Stage* and *Acceleration Stage*.

of an high-power (200 kW) HPT for interplanetary missions.[10,11] In 2003, the Double Layer phenomena has been investigated at the Australian National University as the principal acceleration mechanism of HPTs.[12] At the University of Padova, a 50 W HPT has been designed, developed, and tested during the HPH.COM project,[2] a 1 kW thruster is under development in the frame of the SAPERE-STRONG project,[8] while a propulsion platform for CubeSats[13] is currently in progress in collaboration with Technology for Propulsion and Innovation S.r.l. (T4i),[14] a spin-off of the above-mentioned university. Other research centers have worked on the HPT propulsion concept, namely: the Madrid University,[15] the Tokyo University,[16] the Massachusetts Institute of Technology,[17] the Michigan Institute of Technology,[18] and the Washington University.[19]

In order to optimize the propulsive figures of merit (e.g. specific impulse, thrust/mass ratio, and efficiency) of a HPT, a deep physical insight has to be gained into both the plasma generation and plasma acceleration mechanisms. The dense plasma ($\geq 10^{19}$ m^{-3}) production is governed by the propagation of whistler waves in the discharge region (identified as *Production Stage* in Fig. 1). More specifically, the key physical phenomena that govern the Helicon source are the EM wave propagation, the plasma transport, and their mutual coupling. The acceleration and detachment phenomena take place principally downstream the Helicon source (identified as *Acceleration Stage* in Fig. 1). The *Acceleration Stage* is characterized by the formation of a plume where the plasma is more rarefied than in the *Production Stage* (density in the range 10^{16} - 10^{18} m^{-3}).[20] The plume can be divided into two separate regions, respectively near region and far region, depending on the phenomena which govern the plasma dynamics.[21] In the near region, particle collisions and the geometry of the applied magneto-static field drive the plasma behaviour. Instead in the far region, the expansion of the plasma is mainly governed by the thermal pressure, and the ambipolar diffusion.

Provided the complexity and the variety of the phenomena involved in the dynamics of a HPT, several theoretical and numerical strategies have been adopted to predict the performances of such a thruster. Three analytical models have been developed respectively by Lafleur,[22] Ahedo,[23] and Fruchtmann.[24] These very tools are particularly useful in the preliminary design of the thruster; nonetheless, for the optimization more advanced numerical instruments must be adopted. Several numerical approaches have been pursued in literature for modelling both the *Production Stage* and the *Acceleration Stage*; the most relevant are: fluid,[25] kinetic,[26,27] Particle-In-Cell with Monte-Carlo Collisions (PIC-MCC),[28,29] and hybrid.[20]

This work is devoted to:

- the description of a numerical model of a HPTs which relies on (i) the fluid code 3-Dimensional adVanced fluId dRifT diffUsion plaSma (3D-VIRTUS)[30] for the simulation of the *Production Stage*, and (ii) an analytical model of the plume[22] for the solution of the *Acceleration Stage*, and in turn for the preliminary estimation of the propulsive performances (e.g., thrust and specific impulse).
- the presentation of a combined numerical/experimental campaign performed on a non-optimized low power (50 W range) HPT prototype; the latter is intended to verify the reliability of the code when handling real-life prototypes

Specifically, in Sec. II the numerical methodology is presented. In Sec III the thruster at hand and the measurement setup are described. The results of the combined numerical and experimental campaign are depicted and compared in Sec. IV. Finally, conclusions are drawn in Sec. V.

II. Numerical methodology

The RF antenna, the plasma discharge, along with any additional components (e.g., dielectric vessel, electromagnets, conducting shields), either metallic or dielectric have been included in the model of the Helicon source. Moreover, an arbitrary geometry of the RF antenna, of the discharge tube, and of the confining magneto-static field can be handled. In particular, a preliminary estimations of the propulsive performances can be obtained only if the magnetic nozzle can be treated with the paraxial approximation.[24]

A. 3D-VIRTUS model

The transport problem is solved for an inhomogeneous weakly-ionized argon plasma, that is comprised of a multi-species mixture of electrons, and heavy species (i.e., ions, and neutral particles). Maxwellian distribution function and Drift-Diffusion (DD) approximation have been assumed for each species. The heavy species temperature is considered constant in time, homogeneous, and equal to $T_0 = 600$ K.[31] The resultant set of governing equations comprises Poisson (Eq. 1), energy for the electrons (Eq. 2), and continuity for each species (Eq. 3)

$$\nabla^2 \phi = -q \left(\frac{n_i - n_e}{\varepsilon_0} \right) \tag{1}$$

$$\frac{\partial n_\varepsilon}{\partial t} + \nabla \cdot \mathbf{\Gamma}_\varepsilon + \mathbf{E}_{DD} \cdot \mathbf{\Gamma}_e = R_\varepsilon \tag{2}$$

$$\frac{\partial n_k}{\partial t} + \nabla \cdot \mathbf{\Gamma}_k = R_k \tag{3}$$

In particular, ϕ is the potential generated by charge imbalance, q is the elementary charge, ε_0 the vacuum permittivity, and $\mathbf{E}_{DD} = -\nabla\phi$. n_ε is the electron energy density, and n_k is the number density where $k = e, i, 0, s$ stands respectively for electrons, ions, neutrals, and excited. For what concerns the particles source/sink term R_k, it depends on the chemical reactions considered.[30,32] While the energy source/sink terms R_ε depends on both the energetic balance of chemical reactions ($\mathcal{E}_{\text{chem}}$) and the RF power deposited into the plasma ($\mathcal{E}_{pow}$), specifically $R_\varepsilon = \mathcal{E}_{\text{chem}} + \mathcal{E}_{\text{pow}}$. The DD fluxes for the electron energy ($\mathbf{\Gamma}_\varepsilon$), the electrons ($\mathbf{\Gamma}_e$) and ions ($\mathbf{\Gamma}_i$) are formulated classically.[30] On the contrary, for the neutral and the excited species

$$\mathbf{\Gamma}_0 = D_0 \nabla n_0 + n_0 \mathbf{u} \tag{4}$$

$$\mathbf{\Gamma}_s = D_s \nabla n_s + n_s \mathbf{u} \tag{5}$$

where D_0 (D_s) is the neutral (excited) diffusion coefficient,[30] and $\mathbf{u}$ is the convective speed due to the mass outflow ($\dot{m}_0$).[33] The convective speed has been assumed equal to

$$|\mathbf{u}| = \frac{1}{4} v_{\text{th}} \tag{6}$$

where $v_{\text{th}} = \sqrt{8 k_B T_0 / \pi M}$ is the average thermal speed of the heavy species, k_B is the Boltzmann constant, and M is the heavy species mass. Equation 6 holds true if the neutral gas can be treated as a fluid regime in the production stage, namely $\dot{m}_0 = M(n_0 + n_s)|\mathbf{u}|$, and is in the molecular regime downstream the source outlet, $\dot{m}_0 = 1/4 M(n_0 + n_s) v_{\text{th}}$. For mass conservation, equation 6 holds exactly true at the source outlet.

A Dirichlet boundary condition has been assumed for the solution of equation 1 (Poisson), namely both the walls[34] of the discharge and the source outlet[4] are considered at ground

$$\phi = 0 \tag{7}$$

A Robin condition which enforces the Bhom sheath criterion, has been adopted in all the boundaries of the discharge for equation 1 (electron energy), and for the continuity of electrons and ions.[30] Finally, a Neumann condition is adopted for the continuity equation of both neutral and excited

$$\frac{\partial n_k}{\partial x_\perp} = -\frac{\Gamma_\perp}{D_k} \tag{8}$$

where $\Gamma_\perp$ is the particles flux toward the boundary. In particular, for the excited species $\Gamma_\perp = \Gamma_s = 1/2 n_s v_{\mathrm{th}}$ on the walls of the discharge[35] and $\Gamma_\perp = 0$ at the source outlet. Similarly for the neutrals, $\Gamma_\perp = 0$ at the outlet, and $\Gamma_\perp = -(\Gamma_i + \Gamma_s)$ at the walls.[34]

B. Plume model

An analytical *plume model*,[22] which gives a quasi-1D-axial description of the *Acceleration Stage*, has been adopted to preliminary estimate the propulsive performances. It is based on the assumption that at the source outlet both the electrons and ions enforce the Bhom sheath criterion. Moreover, the magneto-static field in the nozzle region is described with the paraxial approximation.[24] Finally, the position in which the plasma detaches from the magneto-static field is assumed to occur when the ion gyroradius is equal to the radius of the plasma flow area defined by the diverging field lines.[22]

Therefore, the thrust provided by the plasma outflow is

$$F_0 = 2q \int n_e T_e dA \tag{9}$$

where the integration is performed on the source outlet section. Downstream the outlet an additional momentum is delivered to the plasma due to the magnetic nozzle effect. Therefore the total thrust provided by the plasma acceleration is equal to

$$F_p = \frac{\mathcal{M}_{\mathrm{det}}^2 + 1}{2\mathcal{M}_{\mathrm{det}}} F_0 \tag{10}$$

where $\mathcal{M}_{\mathrm{det}}$ is the magnetic Mach number at the detachment point.[22] The latter is assumed to be related to the demagnetization of the electrons;[25,36] namely it occurs in the axial section in which the electron gyroradius (r_e^C) and the radius of the outlet section (R) are equal $r_e^C = R$. The thrust produced by a HPT is obtained summing the contributions due to the plasma acceleration (F_p) and neutral gas expansion (F_{gas}). The latter can be computed as[22]

$$F_{gas} = \dot{m}_0 |\mathbf{u}| + k_B n_0 T_0 A_0 \tag{11}$$

where A_0 is the outlet section. Therefore, the thrust T and the specific impulse I_{sp} are computed as

$$T = F_p + F_{gas} \tag{12}$$

$$I_{sp} = \frac{T}{g_0 \dot{m}_0} \tag{13}$$

where g_0 is the acceleration of gravity at the sea level, and $\dot{m}_0$ is calculated as

$$\dot{m}_0 = M \int (n_0 + n_s)\, dA \tag{14}$$

C. Solution

In the solution of the HPT: (i) first, the Helicon source is resolved with 3D-VIRTUS, (ii) second, thrust and specific impulse are estimated with the *plume model* which takes as input the plasma profiles calculated at the source outlet by 3D-VIRTUS (see figure 2). The numerical solution of the *plume model* is trivial, provided that it involves only algebraic equations.

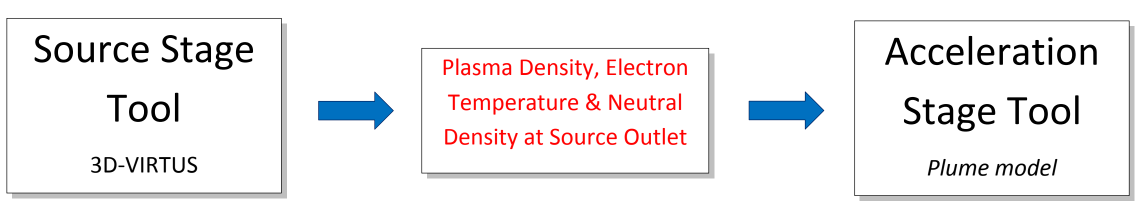

Figure 2. Scheme of the HPT simulation strategy.

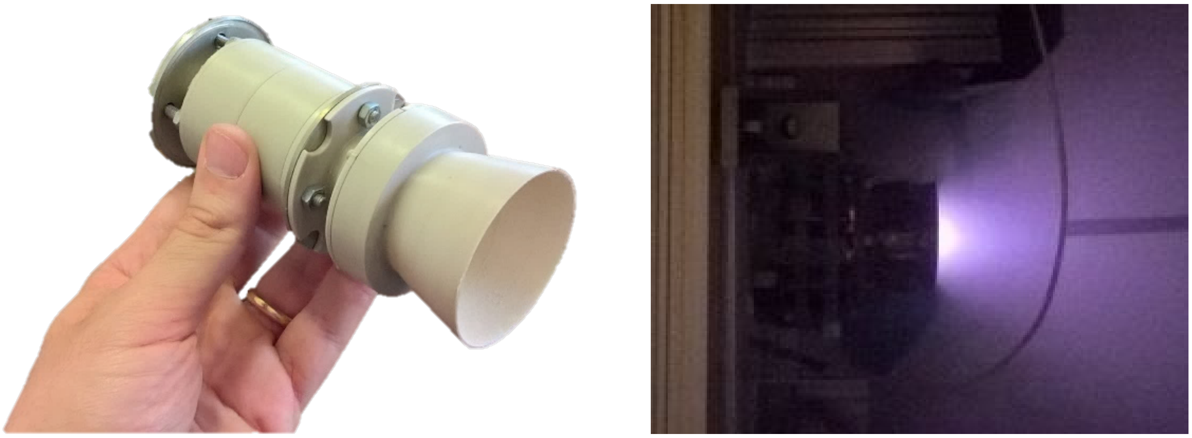

(a) (b)

Figure 3. (a) Picture of the low power (50 W range) HPT prototype under analysis, (b) thruster fastened to the stand and operated with argon propellant.

III. Experimental setup description

A. Thruster

The low-power (50 W range) HPT prototype under consideration (see Fig. 3) has a cylindrical envelope of diameter 55 mm and length 120 mm, its mass is roughly 0.4 kg. The discharge chamber has been realized in hexagonal Boron Nitride (hBN), the RF antenna is a S-Helicon type,[37] and the magneto-static field is generated with two rings of permanent magnets in Samarium Cobalt. The field lines of the resulting magneto-static field has been depicted in Fig. 4; two cusp regions inside the discharge chamber can be noticed. The structure in which the magnets are encased, along with the physical nozzle have been realized in PEEK. Finally, the frame of the prototype is realized in Al and is electrically grounded.

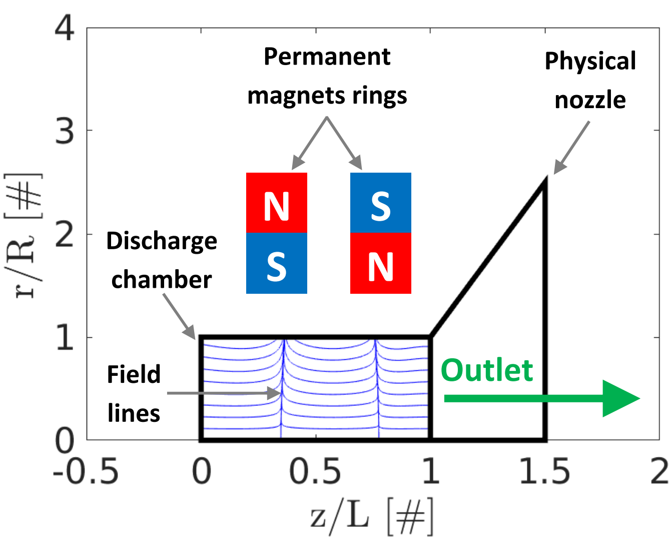

Figure 4. Schematic of the magnetic configuration of the HPT prototype under test. Highlighted the walls of the discharge chamber, the walls of the physical nozzle, the source outlet, the polarization of the two rings of permanent magnets which generate the magneto-static field, along with the field lines inside the discharge chamber. The radial coordinate r is normalized in respect to the source radius R, and the axial coordinate z in respect to the source length L.

B. Measurements system

The thruster performances have been measured at the CISAS high vacuum facility, where the thruster has been tested inside a 2 m long cylindrical vacuum chamber with an inner diameter of 0.6 m, connected to a pumping system with a capacity of 12600 l/s of N_2.[38] The RF power has been provided to the thruster by a water-cooled ENI OEM-12B3-02 linear amplifier driven by a HP 8648A signal generator. A MKS 1179A mass flow controller, whose accuracy is ± 0.01 mg/s, has been employed to regulate the propellant flow injected into the discharge chamber.[39] The equipment employed for the characterization of the thruster includes a thrust balance, specifically designed for RF thrusters of small-to-medium size,[40] and RF probes for vector voltage and current measurement.[39] The former determines the thrust and specific impulse generated with an uncertainty of 10-20 %, whereas the latter allows to monitor the net power provided by the amplifier to the RF antenna of the thruster with an uncertainty of few percentage points. In particular, the thrust balance is calibrated by means of known masses and the uncertainty is calculated with a Monte Carlo algorithm which accounts for the zero-position drift induced by the thermal gradients.

IV. Results

The performances of the thruster (i.e., thrust T and specific impulse I_{sp}) have been evaluated, both experimentally and numerically, for an input power Pw varying from 10 W up to 70 W, and an argon mass flow rate $\dot{m}_0$ from 0.06 mg/s up to 0.15 mg/s.

A. Experimental measurements

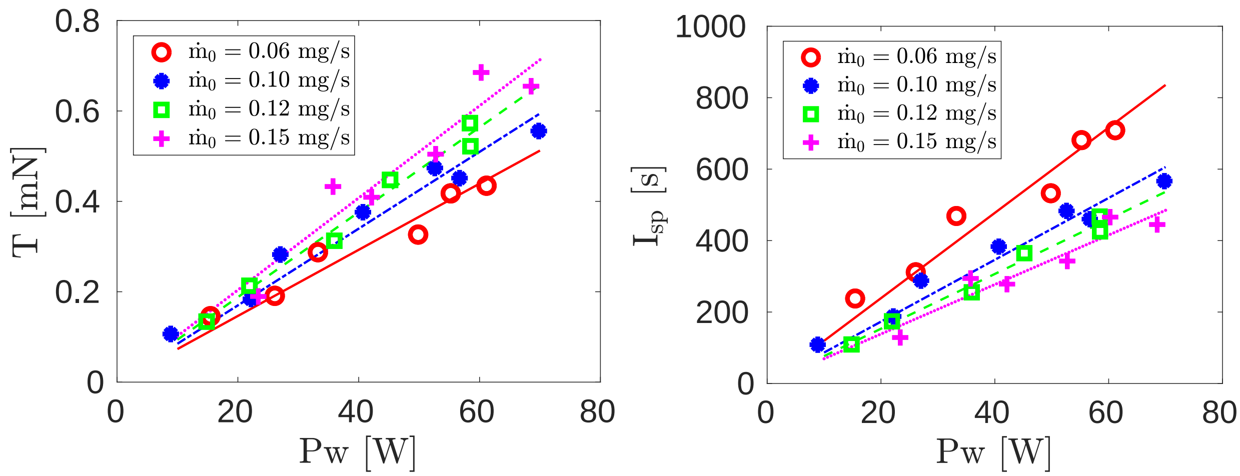

(a) (b)

Figure 5. Experimental measurements of the performances of the HPT prototype operated with argon propellant: (a) thrust T (uncertainty in the order of 15%), and (b) specific impulse I_{sp} (uncertainty in the order of 15-20%) against input power Pw (uncertainty few percent points) for different propellant mass flow rates $\dot{m}_0$.

The results of the testing campaign has been reposted in Fig. 5. Higher (lower) thrust can be obtained with higher (lower) mass flow rates and input power (see Fig. 5(a)). The highest thrust achieved is around $T = 0.8$ mN for an input power of roughly $Pw = 70$ W and a mass flow rate of $\dot{m}_0 = 0.15$ mg/s. The specific impulse depends linearly from the input power and is inverse proportional to the mass flow rate (see Fig. 5(b)). The maximum specific impulse achieved is roughly $I_{sp} = 800$ s with input power of $Pw = 60$ W and a mass flow rate of $\dot{m}_0 = 0.06$ mg/s. No instability issues have been encountered within this input power and mass flow rate ranges. The uncertainty associated to the measurements is in the range of 15% for the thrust, and 15-20% for the specific impulse.

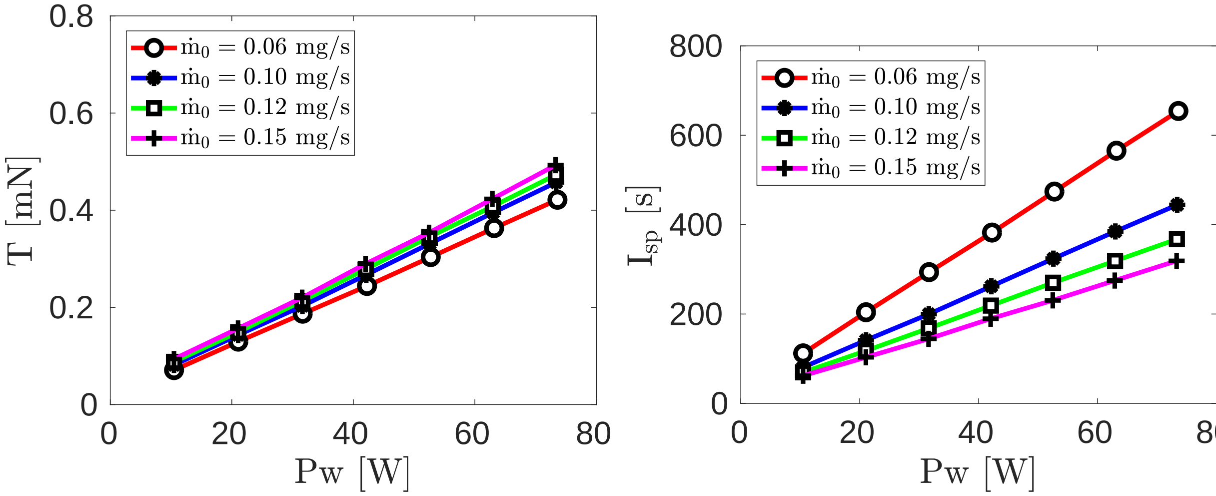

(a) (b)

Figure 6. Numerical estimations of the performances of the HPT prototype operated with argon propellant: (a) thrust T, and (b) specific impulse I_{sp} against input power Pw for different propellant mass flow rates $\dot{m}_0$.

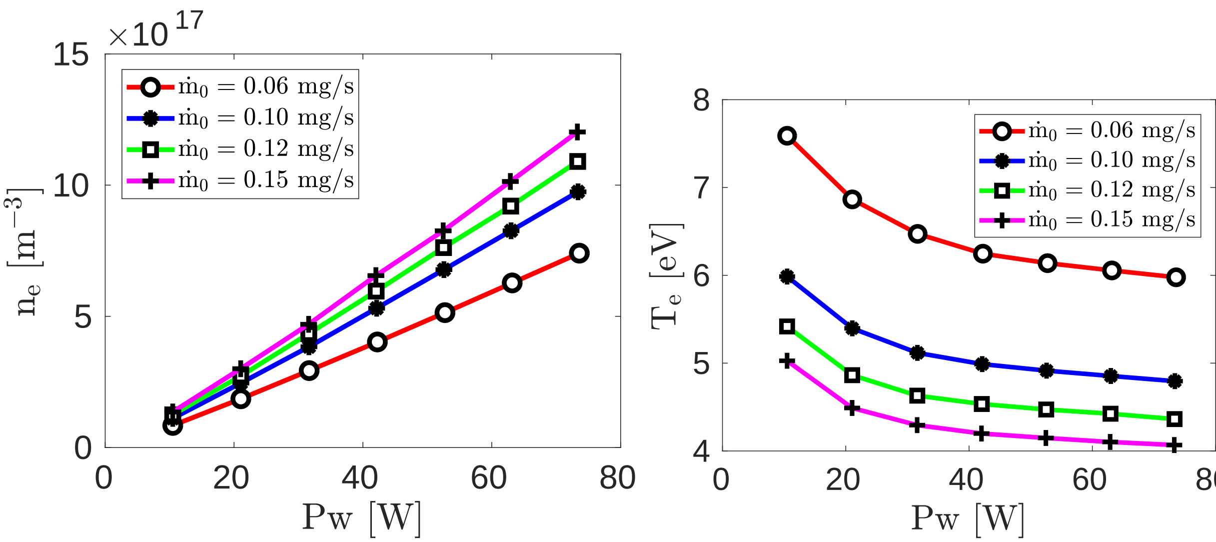

(a) (b)

Figure 7. Numerical estimations of the average plasma properties at the outlet section of the HPT prototype operated with argon propellant: (a) electrons density n_e, and (b) electrons temperature T_e against input power Pw for different propellant mass flow rates $\dot{m}_0$.

B. Numerical estimations

The low-power HPT prototype has been simulated with 3D-VIRTUS for the analysis of the discharge chamber and a plume model for the preliminary estimation of the thruster performances. The plasma transport has been resolved in a 2D domain in order to reduce the computational cost.

The estimation of the thruster performances has been reported in Fig. 6. Higher (lower) thrust is associated to higher (lower) values of mass flow rate and input power (see Fig. 6(a)). The highest thrust estimated is roughly $T = 0.5$ mN for an input power of $Pw = 70$ W and a mass flow rate of $\dot{m}_0 = 0.15$ mg/s. The specific impulse depends linearly from the input power and is inverse proportional to the mass flow rate (see Fig. 6(b)). The maximum specific impulse estimated is roughly $I_{sp} = 600$ s with input power of $Pw = 70$ W and mass flow rate of $\dot{m}_0 = 0.06$ mg/s.

In order to get a deeper physical insight on the results depicted in Fig. 6, it is worth discussing more thoroughly the data provided by 3D-VIRTUS on the plasma discharge. In Fig. 7 the average values of electrons density n_e and electrons temperature T_e on the outlet section of the discharge have been reported. In fact, the thrust provided by the acceleration of the plasma, and in turn T, depends linearly from both n_e and T_e (see Eq. 9). The electrons density increases with the input power, while the electrons temperature mildly decreases (see respectively Fig. 7(a) and Fig. 7(b)); the former effect is more intense than the latter, therefore both thrust and specific impulse increase with the input power (as depicted in Fig. 6). Similarly, the electrons density increases with the mass flow rate while the electrons temperature decreases (see respectively Fig. 7(a) and Fig. 7(b)). The former effect is slightly more intense than the latter and therefore, in combination with an higher thrust provided by the neutral gas acceleration, the total thrust T increases with the mass flow rate (see Fig. 6(a)). On the contrary the specific impulse decreases with the mass flow rate as the electrons temperature does (see Fig. 6(b) and Fig. 7(b)).

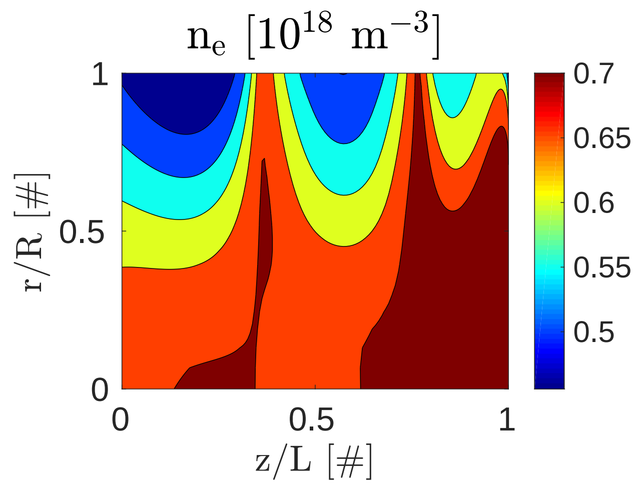

(a)

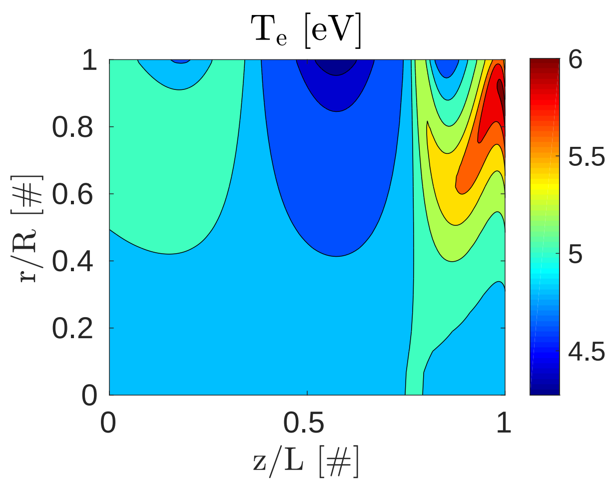

(b)

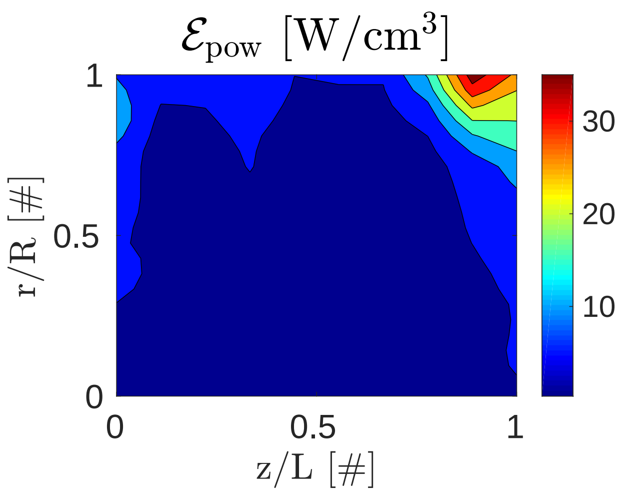

(c)

Figure 8. Numerical estimations of the plasma parameters distribution inside the discharge chamber in function of the radial r and axial z positions (normalized in respect the the source radius R and length L): (a) electron density n_e, (b) electron temperature T_e, and (c) power deposition $\mathcal{E}_{pow}$. Input power $Pw = 50$ W, argon mass flow rate $\dot{m}_0 = 0.10$ mg/s.

Finally, the distribution of the plasma parameters on the discharge chamber, calculated with 3D-VIRTUS, has been depicted on Fig. 8. Specifically, the electrons density n_e, the electrons temperature T_e, and the power deposition $\mathcal{E}_{pow}$ have been reported for an input power $Pw = 50$ W and a mass flow rate $\dot{m}_0 = 0.10$ mg/s. Despite the presence of the two magnetic cusps, the electron density distribution is mildly non-uniform inside the discharge, and the peak value is registered in correspondence of the source outlet (see Fig. 8(a)). The electrons temperature presents a higher degree of non-uniformity in respect to the electrons density, nonetheless the peak value is located in correspondence of the source outlet and close to the edge (see Fig. 8(b)). Moreover, it must be noticed that also the power deposition peak is located very close to the source outlet and on the edge (see Fig. 8(c)). Therefore, even if the prototype has not undertook a dedicated optimization campaign, the plasma parameters are maximum in correspondence of the source outlet leading to an enhancement of the thruster performances (see Eq. 9) in respect to the wall losses.[22] In conclusion, the plasma parameters distributions share the same features highlighted for the case reported in Fig. 8 regardless the value of the input power and of the mass flow rate.

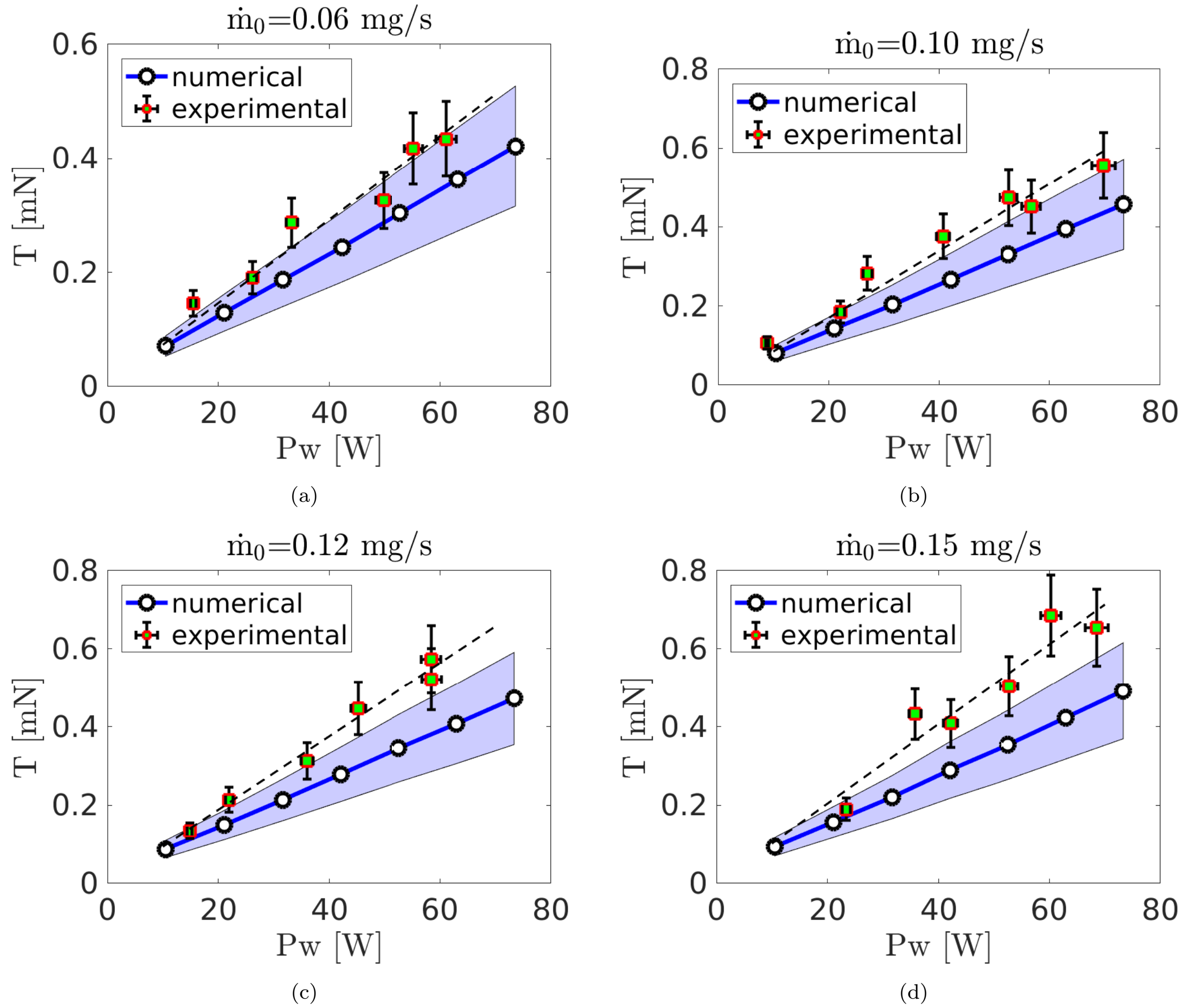

(a) (b) (c) (d)

Figure 9. Comparison between the experimental measurements and the numerical estimations of the attainable thrust T against the input power Pw. Argon mass flow rate: (a) $\dot{m}_0 = 0.06$ mg/s, (b) $\dot{m}_0 = 0.10$ mg/s, (c) $\dot{m}_0 = 0.12$ mg/s, (d) $\dot{m}_0 = 0.15$ mg/s. Uncertainty bands reported for both numerical and experimental results.

C. Comparison

The thruster performances measured experimentally, and estimated numerically have been compared in order to verify the reliability of the HPT model when handling a real-life prototype.

From a qualitative standpoint, the numerical and experimental data show a good agreement. In fact, the HPT model has predicted: (i) the linear dependency of both the thrust T and the specific impulse I_{sp} from the input power Pw (compare Fig. 5 and Fig. 6), (ii) the linear increase of T with the mass flow rate $\dot{m}_0$ (compare Fig. 5(a) and Fig. 6(a)), and (iii) the inverse proportionality between I_{sp} and $\dot{m}_0$ (compare Fig. 5(b) and Fig. 6(b)).

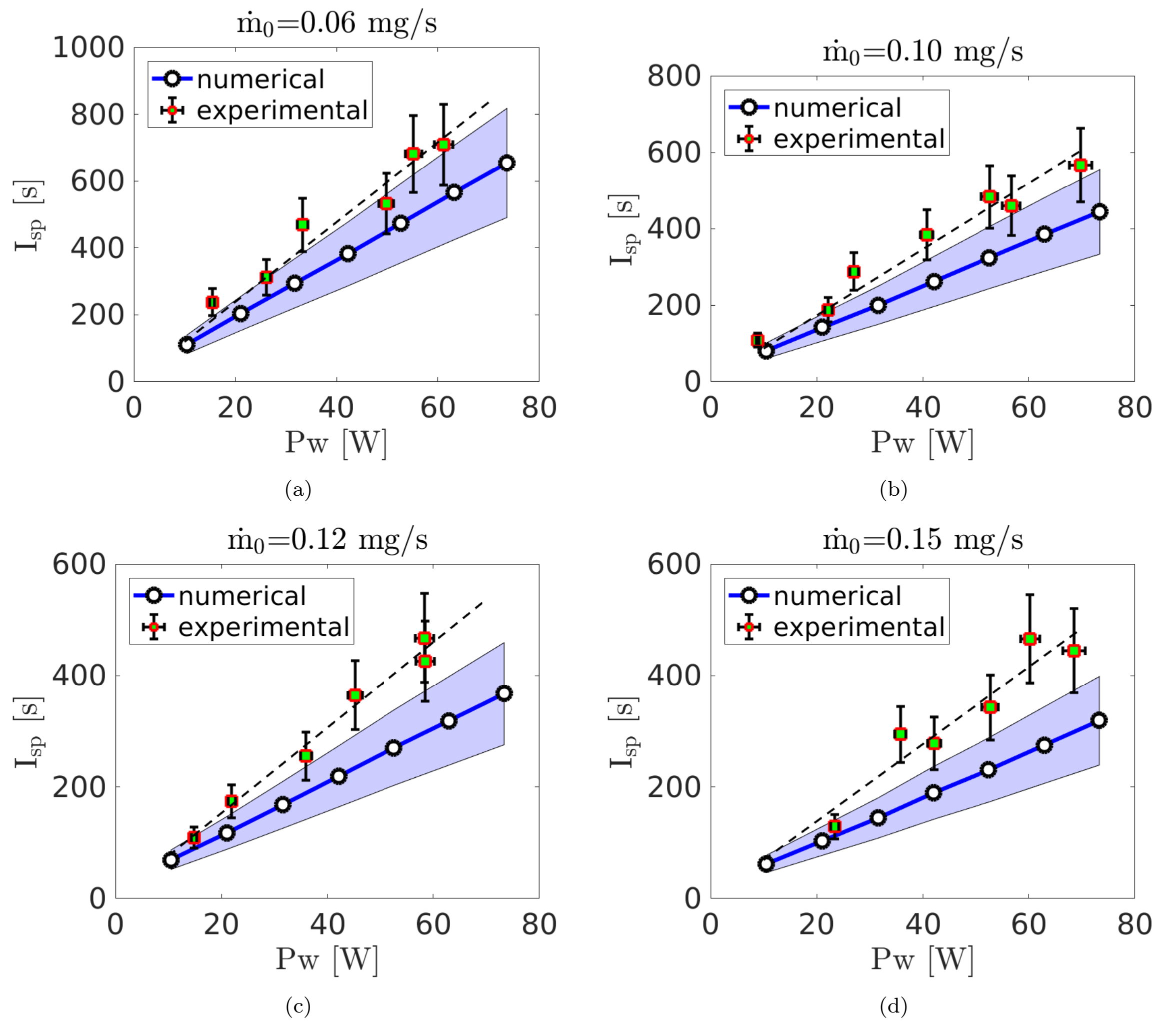

Figure 10. Comparison between the experimental measurements and the numerical estimations of the attainable specific impulse I_{sp} against the input power Pw. Argon mass flow rate: (a) $\dot{m}_0 = 0.06$ mg/s, (b) $\dot{m}_0 = 0.10$ mg/s, (c) $\dot{m}_0 = 0.12$ mg/s, (d) $\dot{m}_0 = 0.15$ mg/s. Uncertainty bands reported for both numerical and experimental results.

From a quantitative standpoint, the agreement is satisfactory. Regardless the value of $\dot{m}_0$, the numerical estimation of T almost agrees with the experimental data for $Pw = 10$ W; however the relative error between experimental and numerical results increases progressively up to 30% for $Pw = 70$ W (see Fig. 9). Similarly, the relative error on I_{sp} grows from few percent point at $Pw = 10$ W up to 30% at $Pw = 70$ W, still regardless the value of $\dot{m}_0$ (see Fig. 10). The mismatching between numerical and experimental data can be attributed to different factors. First, the measurement uncertainty is in the order of 15-20% for both T and I_{sp}, namely it is comparable with the error committed by the numerical predictions. Second, many criteria for the location of the detachment point has been formulated in literature. For example, the mismatching between numerical and experimenal data whould increase up to 40% assuming that the detachment occurs when the ions are demagnetized.[22] At the same time, the mismatching is reduced (increased) up to 25% (35%) assuming that the electrons are demagnetized for $r_e^C = 2R$ ($r_e^C = 0.5R$). Third, in a previous work,[30] it has been demonstrated that the results of 3D-VIRTUS are affected by an uncertainty band of $\pm 20\%$. Fourth, the *plume model* gives a simplified quasi-1D-axial description of the acceleration phenomenon, therefore it is intended for a preliminary estimation of the thruster performances. In conclusion, from the superposition of the error bands depicted in Fig. 9 and Fig. 10, it can be inferred that the quantitative disagreement between numerical and experimental results is comparable with the uncertainty associated to the reference measurements (15-20%) and to the theroetical models (20-30%).

V. Conclusions

In summary, a numerical model of a HPT has been presented which relies on the 3D-VIRTUS code for the accurate solution of the *Production Stage* and on an analytical *plume model* for the *Acceleration Stage* and a preliminary evaluation of the propulsive performances (e.g., thrust and specific impulse). Moreover, a low-power (50 W range) HPT operated with argon gas has been analysed both numerically and experimentally. The comparison has shown a good qualitative and a satisfactory quantitative agreement (disagreement up to 30%). Nonetheless, a better accord was not expected since the plume model adopted for the estimation of the performances is very simplified. Moreover, it has been shown numerically that, even if the thruster is not optimized, the plasma parameters distributions are more intense in the source outlet leading to an enhancement of the propulsive performances in respect to the wall losses.

References

[1]R. J. Cybulski, D. M. Shellhammer, R. R. Lovell, E. J. Domino, J. T. Kotnik, J. Cybulski, R. R. Loveli, Results from SERT I Ion Rocket Flight Test, Tech. Rep. D-2718, NASA (1965).

[2]D. Pavarin, F. Ferri, M. Manente, D. Rondini, D. Curreli, Y. Guclu, M. Melazzi, S. Suman, G. Bianchini, Helicon Plasma Hydrazine: COmbined Micro project overview and development status, in: Proceedings of the 2^{nd} Space Propulsion Conference, no. SP2010-1842379, San Sebastian, ES, 2010.

[3]F. F. Chen, Helicon discharges and sources: a review, Plasma Sources Science and Technology 24 (1) (2015) 014001.

[4]E. Ahedo, M. Merino, Two-dimensional supersonic plasma acceleration in a magnetic nozzle, Physics of Plasmas 17 (7) (2010) 073501.

[5]F. F. Chen, D. Arnush, Generalized theory of helicon waves. i. normal modes, Physics of Plasmas 4 (9) (1997) 3411–3421.

[6]F. F. Chen, Helicon plasma sources, `http://www.seas.ucla.edu/ ffchen/Publs/Chen155R.pdf`, accessed: 2018-09-19.

[7]D. M. Goebel, I. Katz, Fundamentals of electric propulsion: Ion and Hall thrusters, JPL Space Science & Technology Series, 2008.

[8]F. Trezzolani, M. Manente, A. Selmo, D. Melazzi, M. Magarotto, D. Moretto, P. De Carlo, M. Pessana, D. Pavarin, Development and test of an high power RF plasma thruster in project SAPERE-STRONG, in: 35^{th} International Electric Propulsion Conference, no. IEPC-2017-462, Atlanta GA, USA, 2017.

[9]F. Trezzolani, M. Manente, E. Toson, A. Selmo, M. Magarotto, D. Moretto, F. Bosi, P. De Carlo, D. Melazzi, D. Pavarin, Development and testing of a miniature helicon plasma thruster, in: 35^{th} International Electric Propulsion Conference, no. IEPC-2017-519, Atlanta GA, USA, 2017.

[10]F. R. C. Diaz, The VASIMR rocket, Scientific American 283 (5) (2000) 90–97.

[11]B. W. Longmier, J. P. Squire, L. D. Cassady, M. G. Ballenger, M. D. Carter, C. Olsen, A. V. Ilin, T. W. Glover, G. E. McCaskill, F. C. Dıaz, et al., Vasimr vx-200 performance measurements and helicon throttle tables using argon and krypton, in: 32^{nd} International Electric Propulsion Conference, no. IEPC-2011-156, Wiesbaden, DE, 2011.

[12]R. W. Boswell, C. Charles, The helicon double layer thruster, in: 28^{th} International Electric Propulsion Conference, no. IEPC-2003-332, Toulouse, FR, 2003.

[13]M. Manente, F. Trezzolani, M. Magarotto, E. Fantino, A. Selmo, N. Bellomo, E. Toson, D. Pavarin, Regulus: A propulsion platform to boost small satellite missions, Acta Astronautica 157 (2019) 241–249.

[14]Technology for propulsion and innovation official web site, `http://www.t4innovation.com/`, accessed: 2018-09-19.

[15]M. Merino, J. Navarro, S. Casado, E. Ahedo, V. Gómez, M. Ruiz, E. Bosch, J. G. del Amo, Design and development of a 1 kw-class helicon antenna thruster, in: 34^{th} International Electric Propulsion Conference, no. IEPC-2015-297, Kobe, J, 2015.

[16]S. Shinohara, H. Nishida, T. Tanikawa, T. Hada, I. Funaki, K. P. Shamrai, Development of electrodeless plasma thrusters with high-density helicon plasma sources, IEEE Transactions on Plasma Science 42 (5) (2014) 1245–1254.

[17]O. V. Batishchev, Minihelicon plasma thruster, IEEE Transactions on plasma science 37 (8) (2009) 1563–1571.

[18]J. P. Sheehan, T. A. Collard, F. H. Ebersohn, B. W. Longmier, Initial operation of the cubesat ambipolar thruster, in: 34^{th} International Electric Propulsion Conference, no. IEPC-2015-243, Kobe, J, 2015.

[19]T. Ziemba, J. Carscadden, J. Slough, J. Prager, R. Winglee, High power helicon thruster, in: 41^{st} AIAA/ASME/SAE/ASEE Joint Propulsion Conference & Exhibit, no. AIAA 2005-4119, Tucson AZ, USA, 2005.

[20]F. Cichocki, A. Domínguez-Vázquez, M. Merino, E. Ahedo, Hybrid 3d model for the interaction of plasma thruster plumes with nearby objects, Plasma Sources Science and Technology 26 (12) (2017) 125008.

[21]M. Merino, F. Cichocki, E. Ahedo, A collisionless plasma thruster plume expansion model, Plasma Sources Science and Technology 24 (3) (2015) 035006.

[22]T. Lafleur, Helicon plasma thruster discharge model, Physics of Plasmas 21 (4) (2014) 043507.

[23]E. Ahedo, J. Navarro-Cavallé, Helicon thruster plasma modeling: Two-dimensional fluid-dynamics and propulsive performances, Physics of Plasmas 20 (4) (2013) 043512.

[24]A. Fruchtman, K. Takahashi, C. Charles, R. Boswell, A magnetic nozzle calculation of the force on a plasma, Physics of Plasmas 19 (3) (2012) 033507.

[25]E. Ahedo, M. Merino, On plasma detachment in propulsive magnetic nozzles, Physics of Plasmas 18 (5) (2011) 053504.

[26]G. Hagelaar, L. Pitchford, Solving the boltzmann equation to obtain electron transport coefficients and rate coefficients for fluid models, Plasma Sources Science and Technology 14 (4) (2005) 722–733.

[27]M. Martinez-Sanchez, J. Navarro-Cavallé, E. Ahedo, Electron cooling and finite potential drop in a magnetized plasma expansion, Physics of Plasmas 22 (5) (2015) 053501.

[28]M. Manente, J. Carlsson, I. Musso, C. Bramanti, D. Pavarin, F. Angrilli, Numerical simulation of the helicon double layer thruster concept, in: 43^{rd} AIAA/ASME/SAE/ASEE Joint Propulsion Conference & Exhibit, no. AIAA 2007-5312, Cincinnati, OH, 2007.

[29]G. Gallina, M. Magarotto, M. Manente, D. Pavarin, Enhanced bidimensional pic: an electrostatic/magnetostatic particle-in-cell code for plasma based systems, Journal of Plasma Physics 85 (2).

[30]M. Magarotto, D. Melazzi, D. Pavarin, 3D-VIRTUS: Equilibrium condition solver of radio-frequency magnetized plasma discharges for space applications, Computer Physics Communications (to be published).

[31]D. Bose, T. Govindan, M. Meyyappan, Modelling of magnetic field profile effects in a helicon source, Plasma Sources Science and Technology 13 (4) (2004) 553.

[32]M. A. Lieberman, A. J. Lichtenberg, Principles of plasma discharges and materials processing, John Wiley & Sons, Inc., Hoboken NJ, USA, 2005.

[33]M. Abdollahzadeh, J. C. Pascoa, P. J. Oliveira, Implementation of the classical plasma–fluid model for simulation of dielectric barrier discharge (DBD) actuators in OpenFOAM, Computers & Fluids 128 (2016) 77–90.

[34]J. Bukowski, D. Graves, P. Vitello, Two-dimensional fluid model of an inductively coupled plasma with comparison to experimental spatial profiles, Journal of Applied Physics 80 (5) (1996) 2614–2623.

[35]G. Hagelaar, F. De Hoog, G. Kroesen, Boundary conditions in fluid models of gas discharges, Physical Review E 62 (1) (2000) 1452–1454.

[36]M. Merino, E. Ahedo, Plasma detachment mechanisms in a magnetic nozzle, in: 47th AIAA/ASME/SAE/ASEE Joint Propulsion Conference & Exhibit, San Diego, CA, USA, 2011, p. 5999.

[37]S-helicon antenna, international PCT/IB2016/050199 15.01.2016, Italian patent number VR2015A000007 del 16.01.2015.

[38]D. Pavarin, A. Lucca Fabris, F. Trezzolani, M. Manente, M. Faenza, F. Ferri, A. Selmo, K. Katsonis, C. Berenguer, Low power rf plasma thruster experimental characterization, in: Proceedings of the 48^{th} AIAA/ASME/SAE/ASEE Joint Propulsion Conference & Exhibit, AIAA 2012-4191, Atlanta, GA, USA, 2012.

[39]F. Trezzolani, Optimization and automatic control of radio-frequency plasma thrusters for space applications, PhD thesis, Università degli studi di Padova (2015).

[40]F. Trezzolani, M. Magarotto, M. Manente, D. Pavarin, Development of a counterbalanced pendulum thrust stand for electric propulsion, Measurement 122 (2018) 494–501.